Journal of Solid State Chemistry 187 (2012) 134–142

Contents lists available at SciVerse ScienceDirect

Journal of Solid State Chemistry

journal homepage: www.elsevier.com/locate/jssc

Pressure response of vacancy ordered maghemite (γ-Fe_2O_3) and high pressure transformed hematite (α-Fe_2O_3)

Giovanni Hearne [a,*], Vittoria Pischedda [b]

[a] Department of Physics, University of Johannesburg, PO Box 524, Auckland Park, 2006 Johannesburg, South Africa
[b] Laboratoire de Physique de la Matière Condensée et Nanostructures, University Lyon 1 and CNRS, 69622 Villeurbanne Cedex, France

ARTICLE INFO

Article history:
Received 19 September 2011
Received in revised form
31 December 2011
Accepted 1 January 2012
Available online 10 January 2012

Keywords:
Ferric iron oxides
Vacancies
High pressures
Mössbauer spectroscopy
Topotactic transformation
Spin reorientation

ABSTRACT

Combined XRD and Mössbauer effect spectroscopy studies to high pressures of ~30 GPa of vacancy ordered maghemite are presented. The vacancy ordered superstructure is robust and remains intact up to the pressure-induced onset transition to hematite at 13–16 GPa. The pressure transformed hematite is shown to be crystallographically textured, unlike the randomised low pressure maghemite phase. This arises out of a pressure or stress instigated topotactic transformation of the cubic-spinel to hexagonal-corundum structure. The textured sample permits us to obtain information on the spin reorientation behavior of the pressure transformed hematite in compression and decompression sequences. Spin reorientation is restricted to ~15° over wide pressure ranges, attributable to the effect of entrapped vacancies in the high pressure structure. Thus there are structural and magnetic peculiarities specific to pressure transformed hematite not evident in pressurized hematite starting material. These are triggered by the maghemite→hematite transformation.

1. Introduction

Maghemite (γ-Fe_2O_3), the fully oxidized structural analog of magnetite Fe_3O_4, is both of geophysical significance and of crucial importance to the magnetic recording and data storage industries. Other uses are as catalysts, in pigments as well as a large range of biomedical applications.

There has been considerable interest in the magnetic–electronic pressure response of magnetite in the last several years. This has given rise to several publications and what appears to be false alarms based on the claims of an inverse→normal spinel structure change in the low pressure regime, see Baudelet et al. and references therein [1].

The pressure response of maghemite is less well studied, although there has been some X-ray diffraction (XRD) studies of nano-phase maghemite [2,3], and to the best of our knowledge one ^{57}Fe Mössbauer effect spectroscopy (MS) study [4]. It is now established that in the bulk material a sluggish structural transition at room temperature is onset at 10–15 GPa where the low pressure cubic spinel phase starts to transform to the well known corundum structure of hematite α-Fe_2O_3 and reaches completion by 30–35 GPa [2,4].

Hematite as starting material has also been quite extensively studied in high pressure–temperature (P–T) experiments. Much of this is motivated by geo-science considerations of the behavior of these oxides under deep Earth conditions [5]. There has also been extensive interest in the sluggish structural transition at room temperature which is onset at ~50 GPa and where a progressive transformation to the distorted corundum structure (Rh_2O_3-II type) occurs, concurrent with an insulator–metal transition and magnetic collapse [6–8].

All of the above-mentioned oxides are magnetic insulators, typifying strongly correlated 3d transition metal compounds of the charger-transfer type. Pressure tuning the interplay between the spin, charge and even orbital degrees of freedom in these oxides has been considered very topical in recent years [1,6,9].

In this work we make a more detailed examination of the pressure-induced maghemite→hematite transition in a well characterized bulk sample [10]. The existence of the structural transformation at pressure is well known for several years now, our work serves to emphasize the effects and consequences of the transformation on the high pressure phase which has not been delineated in previous studies. It is shown that the response of the pressure transformed hematite has structural and magnetic peculiarities that are not evident when hematite itself, as starting material, is cycled to high pressure and back to ambient conditions again. Thus these peculiarities are supposed to be linked to the pressure or stress instigated structural transformation of the defect cubic spinel (maghemite) to corundum structure of hematite.

* Corresponding author.
E-mail addresses: grhearne@uj.ac.za (G. Hearne), Vittoria.Pischedda@univ-lyon1.fr (V. Pischedda).

0022-4596/$ - see front matter © 2012 Elsevier Inc. All rights reserved.
doi:10.1016/j.jssc.2012.01.003

The pressure response of a high quality sample of maghemite with an ordered vacancy sub-lattice is examined. A comparison is made with other structural studies and the previous ^{57}Fe MS study. This combined XRD structural and MS magnetic study helps to reveal the high degree of lattice preferred orientation in the pressure transformed phase. There is crystallographic *c*-axis alignment and an associated magnetic texturing of moments, biased in the direction of the load axis. Decompression experiments evidence deformation of the local atomic environment of the Fe atom which affects the direction of the maximum value of the electric field gradient (EFG), normally assumed to always be directed along the *c*-axis of the hexagonal unit cell. Probing the textured hematite sample in compression–decompression cycles allows us to obtain unique information on the pressure-response of the spin reorientation angle. This spin reorientation, as a result of competing magnetic anisotropies is shown to be quite different to that associated with the Morin transition in pristine hematite starting materials.

This manuscript is organized as follows : Section 2 has a description of the XRD and ^{57}Fe MS experiments; Section 3 has the results of the XRD pressure studies as well as results of the Mössbauer experiments at pressure together with necessary background theory needed to interpret the data; Section 4 combines the outcomes of the XRD and Mössbauer experiments to rationalize the behavior of the pressure transformed hematite and Section 5 culminates in the conclusions of this study.

2. Experimental

The sample has been obtained from the source in the reference by Shmakov et al. [10]. As detailed in that reference it was prepared as a high purity powder by thermal decomposition of α-FeOOH. The sample has been very well characterized by synchrotron XRD and electron microscopy and is the main subject of the publication by Shmakov et al. [10]. Our XRD and ^{57}Fe MS measurements at ambient conditions confirm the integrity of the samples to be that of single phase maghemite (e.g., see Fig. 1).

Synchrotron XRD experiments at high pressure have been performed in angular dispersive mode (λ=0.7022 Å) at the XRD1 beam line of the ELETTRA Synchrotron (Trieste, Italy) using a miniature piston-cylinder type DAC with anvil culets of 400 μm diameter. The sample has been loaded in a 200 μm diameter cavity in a stainless steel gasket pre-indented to 80 μm thickness. A piece of Pt foil has been used as internal pressure calibrant and we loaded the sample chamber with liquid nitrogen as pressure transmitting medium by an immersion technique involving the opening and sealing of the DAC to low pressures in a cryogen bath. The explored pressure range was from ambient pressure to 30 GPa and back to ambient at intervals of about 2 GPa. The diffractograms were collected at room temperature on a CCD area detector and the images were integrated with the FIT2D software package [11]. These were subsequently analyzed by the GSAS code [12] to extract the cell parameters from a full-profile fitting analysis.

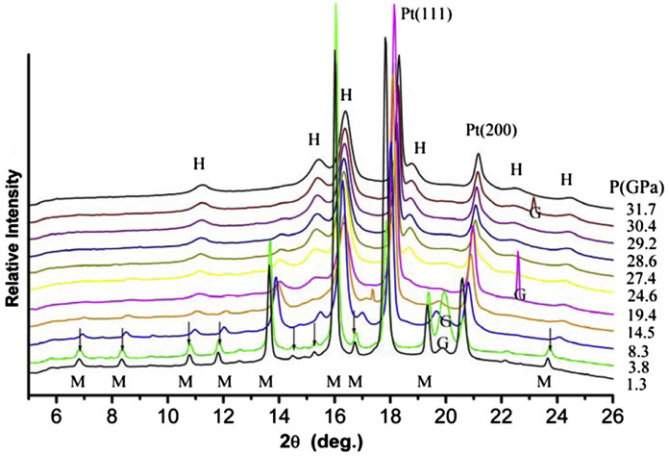

Fig. 1. Selected powder XRD spectra of maghemite up to 32 GPa at room temperature. The maghemite (γ-Fe_2O_3) to hematite (α-Fe_2O_3) transformation is onset in the region 14–19 GPa. The labels denote M (maghemite reflections), H (hematite reflections), Pt (platinum), G (extra peaks: gasket or impurity). The weak superstructure peaks from the vacancy ordering in maghemite are indicated by arrows.

Details of the MS experimental set-up for pressure work, on the natural Fe abundance sample, has been delineated in the reference by Takele and Hearne [13]. A separate but similar piston-cylinder DAC to the XRD work has been used. Similar to the XRD study, the sample was loaded as loose randomized powder grains into a 250 μm diameter cavity of a Re gasket indented to a thickness of ~30 μm. Silicone oil was used as the pressure transmitting medium. The average pressure was determined from the fluorescence spectra of a few ruby balls distributed in the cavity and the pressure distribution never exceeded 5% of the average pressure. Data acquisition times at room temperature were typically 20–40 h to obtain 250,000 counts per channel for a spectrum and its mirror image in 1024 channels. Each spectrum was folded to remove baseline curvature prior to the fitting using the WINORMOS analyzing software [14]. Lorentzian profiles have been used in fitting the sextet spectra involving theoretical considerations where the electric quadrupole interaction is much smaller than the magnetic dipole interaction.

The relative intensities and line width in the typical sextet profile obtained for a thin randomized powder sample of maghemite (10 mg/cm^2) measured outside of the DAC compare favorably with the sample measured in the DAC after closure. This is taken to indicate that so-called thickness (line broadening) effects are not significant for the pressurized sample, and thus the fitting using the usual Lorentzian profiles is reliable [15].

3. Results

3.1. XRD pressure outcomes

Maghemite (γ-Fe_2O_3) is the fully oxidized structural analog of magnetite (Fe_3O_4), but differs from the latter by the presence of vacancies distributed on the cation sublattice, to ensure charge compensation. Its formula can be written $(Fe^{3+})\,[Fe^{3+}_{5/3}\,\square_{1/3}]\,O_4$ where ( ) and [ ] designate tetrahedral and octahedral coordination, respectively. Charge balance is attained by way of vacancies, symbolized by □ and constituting ~11% of the cation sites. The vacancies can be distributed at random (resulting in a cubic unit cell whose space group is *Fd-3m*) or partially ordered on the octahedral positions resulting in a change of the cubic cell (to space group $P4_332$) or, for the fully ordered structure, in the formation of a superlattice involving the vacancies such that the unit cell is best described as tetragonal (space group $P4_12_12$) with lattice parameters $a'=b'\approx a$ and $c'\approx 3a$ [16]. The lattice parameters a',b',c' are for the tetragonal structure while a is the lattice parameter for the cubic structure.

In our sample the presence of weak superstructure reflections in the diffraction pattern at ambient conditions, see Fig. 1, indicates ordering of cation vacancies and its tetragonal superstructure has been well described in previous work [10]. It may be noted that there is no indication of appreciable preferred orientation effects. There is an increased contribution to the background

of the diffraction pattern due to the sample location in the DAC environment and we were not able to distinguish the very weak superlattice reflections (1 0 1) and (1 0 2) at $2\theta < 6^\circ$. These are features of the tripling of the unit cell. In the analysis we are therefore obliged to use a unit cell for the partially ordered structure with $a' = b' = a$, $c' \approx a$ and space group $P4_32_12$ (isomorphic subgroup of $P4_12_12$) for initial trial refinements. The refined structural parameters derived from this space group are then used in a constrained refinement under the $P4_12_12$ space group to derive the final set of structural parameters, as already used by Greaves [17] and Jorgensen et al. [18].

Fig. 1 shows high pressure powder XRD patterns of maghemite up to 32 GPa at room temperature. The original ordered vacancy structure of maghemite is maintained up to at least ~14.5 GPa where we can still distinguish the presence of the weak superlattice reflections. At ~19 GPa additional signatures, at 2θ values of 15° and 19°, are apparent. This suggests that the onset transformation to a new structural phase ascribed to hematite (α-Fe_2O_3) is in the range 14–19 GPa. Maghemite phase signatures coexist with the new structural phase to beyond ~25 GPa and evolve into the background signal by ~30 GPa.

Our results are in good agreement with transition pressures reported in previous XRD studies [19], as well as the ^{57}Fe MS pressure study [4]. On the other hand Jiang et al. [2] and Clark et al. [3] found phase transition pressures at ~25 GPa and well beyond this, for bulk materials. These do not likely represent onset transition pressures but values where the hematite signatures start to become significant. It may be noted that the phase transition in γ-Fe_2O_3 can be affected by the preparation method of the specimen, metal ion doping, particle size, degree of crystallinity of the sample etc.

The pressure-induced phase transformation from maghemite to hematite is irreversible and upon decompression the high pressure form is preserved to ambient conditions. In Fig. 2 we show the hematite patterns from 25.5 GPa to ambient pressure collected upon decompression. Hematite crystallizes in the corundum-type structure with space group *R-3c* and has a rhombohedral primitive unit cell [20]. It can be also described in a hexagonal unit cell setting containing six formula units, which is what we will refer to in the rest of this manuscript [21]. The trigonal axis of the FeO_6 octahedron is directed along the *c*-axis of the hexagonal unit cell. It is along this *c*-axis that Fe atoms in adjacent layers share faces of FeO_6 octahedra [7,20].

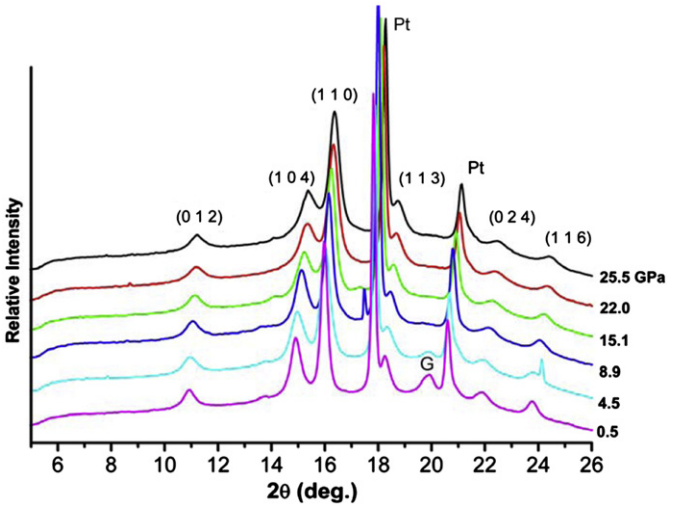

Fig. 2. Powder XRD patterns of the high pressure transformed hematite during decompression.

The lattice constants of the pressure transformed hematite after decompression to ambient conditions have been refined to be, $a = 5.060(5)$, $c = 13.75(2)$ Å and $V = 304.9(8)$ Å^3. The density difference between the maghemite and the hematite phase at ambient conditions is 8.5%. The cell volume and *c*/*a* ratio are plotted in Fig. 3 for the pressure transformed hematite compression and decompression sequences. The *c*/*a* ratio appears to be somewhat erratic on compression as a result of the refinement in a two phase system in which the phase transformation is still evolving to completion at ~30 GPa. The behavior seems to be more regular upon decompression, first weakly monotonically increasing as pressure decreases. In the region of ~7 GPa there appears to be an onset of a discontinuous change. This perhaps signifies some local structural changes (bonding distortions) of the FeO_6 octahedron.

The diffraction patterns of hematite at all pressures during compression and decompression indicate the presence of texture in the sample, even after pressure release to ambient conditions in the compacted sample, see Fig. 4.

In particular the (1 1 0) and (1 0 4) intensity ratio is inverted compared to the pattern of a sample of randomly oriented grains. This is seen in Fig. 4 where there is a comparison of the raw hematite XRD pattern at ambient conditions after decompression with a simulated pattern of randomly oriented grains of hematite. It may be noted that similar lattice preferred orientation behavior

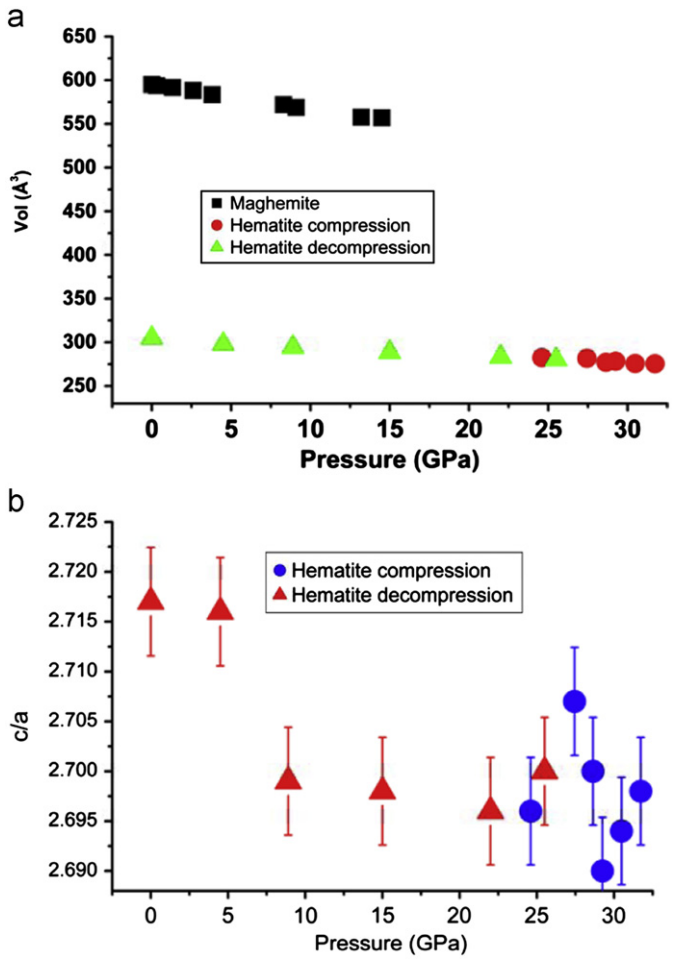

Fig. 3. (a) Variation of the unit cell volume as a function of pressure at room temperature for maghemite (squares) and pressure transformed hematite (circles: compression data; green triangles: decompression data). (b) Variation of the *c*/*a* ratio for the pressure transformed hematite structure in compression and decompression sequences.

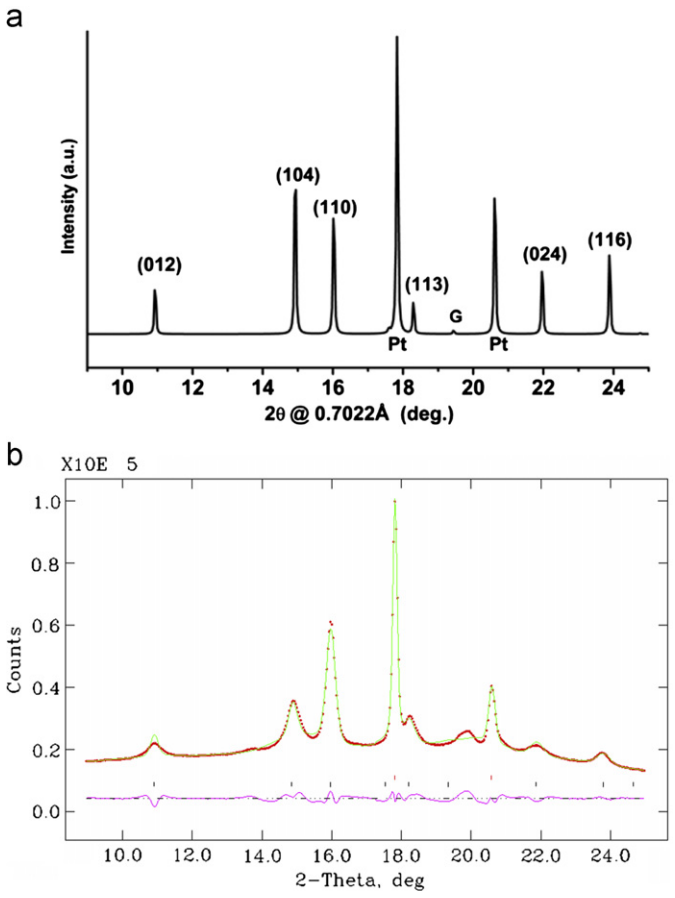

Fig. 4. Top panel shows simulated XRD pattern for randomly oriented hematite+Pt powder sample. Labels are *hkl* values of hematite, Pt (platinum) and G (gasket) reflections. Bottom panel shows observed and calculated XRD patterns for textured hematite at ambient conditions as recovered from high pressure. Rietveld refinement has been performed using a March–Dollase semiempirical function to model the lattice preferred orientation effect. The difference pattern is shown below the fitted spectrum.

is evident in the XRD patterns of recent pressure studies comparing the transformation behavior of bulk and nano-phase maghemite. Yet these preferred orientation effects have not been highlighted or linked to the structural transformation [19].

To refine the structure of the recovered hematite sample we then took into account a preferred orientation correction using the March–Dollase semi-empirical function available in GSAS [22]. The best fit (bottom panel of Fig. 4) is obtained with a preferred orientation of the *c*-axis of hematite such that there is bias along the incident beam (load axis) direction.

3.2. ^{57}Fe MS pressure studies

3.2.1. Maghemite spectra

Fig. 5 shows the relatively high resolution Mössbauer spectra in the pressure regime up to ~20 GPa. The two-site (tetrahedral and octahedral) feature sextet patterns of the spectra are evident from the fitting up to ~13 GPa. At low pressures close to ambient conditions these yield magnetic hyperfine fields, B_{hf}, of 49.4 T and 51.0 T at tetrahedral and octahedral sites, respectively, in accordance with the literature [23]. Beyond 13 GPa a new sextet component (shown shaded and having $B_{hf}=52.2$ T) emerges, indicative of the onset of the second-order maghemite→hematite transformation. This figure suggests that the onset of the phase transition is in the range 13–16 GPa consistent with the XRD data of Fig. 1; but is likely somewhat dependent on the experimental conditions (particle size, pressure transmitting medium etc).

In this low pressure regime the spectra of maghemite have also been fitted with a single sextet to check for the onset of line broadening likely signifying the onset of the structural transition (bottom panel of Fig. 5). Such line broadening is seen to develop at ~13 GPa and is likely the onset pressure of the transformation.

At 16 GPa and beyond where the hematite abundance, deduced from the total absorption area of the spectral component, becomes appreciable ($\geq$33%), unusual relative line intensities start to evolve for the sextet absorption profile. This is seen by focusing on the intensities of adjacent resonances of lines 2 and 3 (ratio I_2/I_3) or lines 5 and 4 (ratio I_5/I_4), where I denotes the absorption intensity or area (see Fig. 5).

3.2.2. Relative intensities of high pressure phase spectra and the Morin transition

For any spectral component the ratio of these lines is dependent on the angle, γ, between the γ-ray propagation direction (which in this case is along the load axis) and the direction of B_{hf} at the ^{57}Fe nucleus (which is collinear with the atomic spin moment). The ratio is given by [24,25],

$$R=\frac{I_{2,5}}{I_{3,4}}=\frac{\sin^2\gamma}{\frac{1}{4}(1+\cos^2\gamma)}, \quad (1)$$

R ranges from zero for $\gamma=0^\circ$ to 4 for $\gamma=90^\circ$ and has a value of 2 at $\gamma\approx 55^\circ$, see Fig. 6(a). An assembly of spins randomly oriented in the sample is expected to give a sextet pattern with relative intensities of 3:2:1:1:2:3. That is, the ratio $R_A=2$ and the subscript A refers to an assembly of spins. Note that a value $R_A=2$ will also be obtained for $\gamma=55^\circ$ for a single crystal sample or one showing preferred orientation. The absorption areas instead of intensities are often used to compare the relative strengths of the resonance lines and are therefore needed to obtain the R_A value. R_A may involve errors due to so-called saturation effects when the sample thickness exceeds certain recommended values [15,26]. The bottom panel of Fig. 5 shows that such effects are expected to contribute negligible error in the evaluation of R_A. That is, the sample measured in the DAC at ambient pressure yields similar spectral parameters to that of a thin absorber of ~10 mg/cm^2 measured outside of the DAC (open symbols).

The fitting of the spectra at $P\geq 19$ GPa involves the pressure transformed hematite component (as a majority phase exceeding 50% abundance) and the maghemite components comprising the tetrahedral and octahedral sites of the spinel structure. The hematite component at these high pressures has values for $R_A\leq 1$, well below that expected for an assembly of randomly oriented spins (in which $R_A=2$). Obtaining the relative line intensities for the minority phase (transforming maghemite) component are more ambiguous because of strong overlap of inner lines 2, 3, 4, 5 (see Fig. 5) and two closely aligned and overlapping octahedral and tetrahedral site spectral components. At these pressures we rather choose to model the transforming maghemite component as a single broadened sextet. The R_A value for this maghemite component may be constrained at ~1.6 similar to the value at the onset of the transformation at low pressure (see bottom panel of Fig. 5) or left as a free fitting parameter. This does not impact significantly on the R_A value obtained for the pressure transformed hematite component in which $R_A\approx 1$. Our attention is focused on this pressure transformed hematite component.

Under ambient conditions hematite is known to undergo a spin reorientation at the so-called Morin transition of $T_M\sim 260$ K. This is a consequence of competing magneto-crystalline and magnetic dipolar anisotropy energies K_{MC} and K_{MD}, respectively,

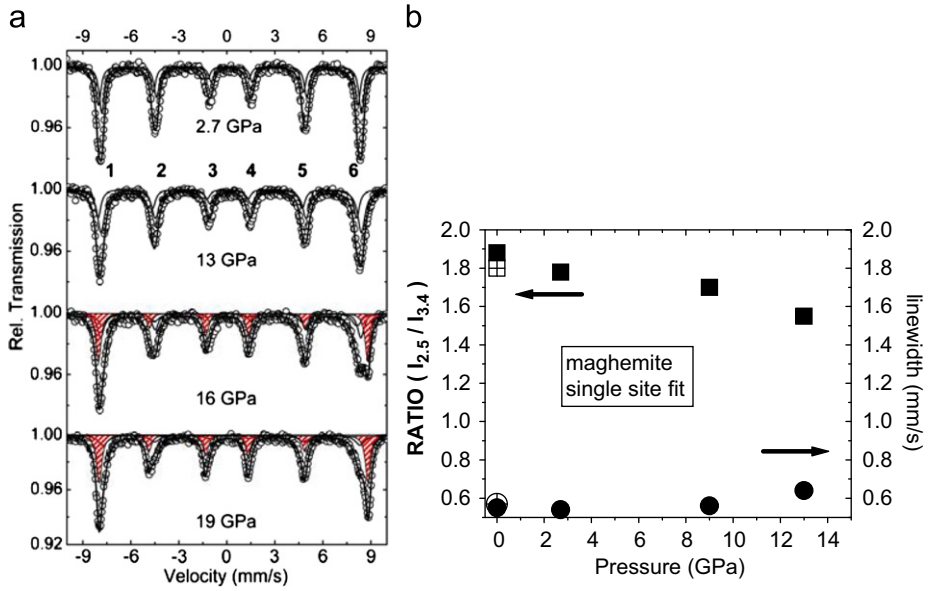

Fig. 5. (a) Mössbauer spectra of maghemite to pressures beyond the onset of the structural transition to hematite. Solid lines through the data (symbols) are the theoretical fit. Hematite component is shown shaded at 16 and 19 GPa. Note the change in relative line intensities in the range 13–16 GPa when the hematite component starts to evolve. Panel (b) shows single component fit to monitor the resonance absorption area ratio R_A and linewidth of the pressurized maghemite. Open symbols are for a thin sample measured outside of the DAC.

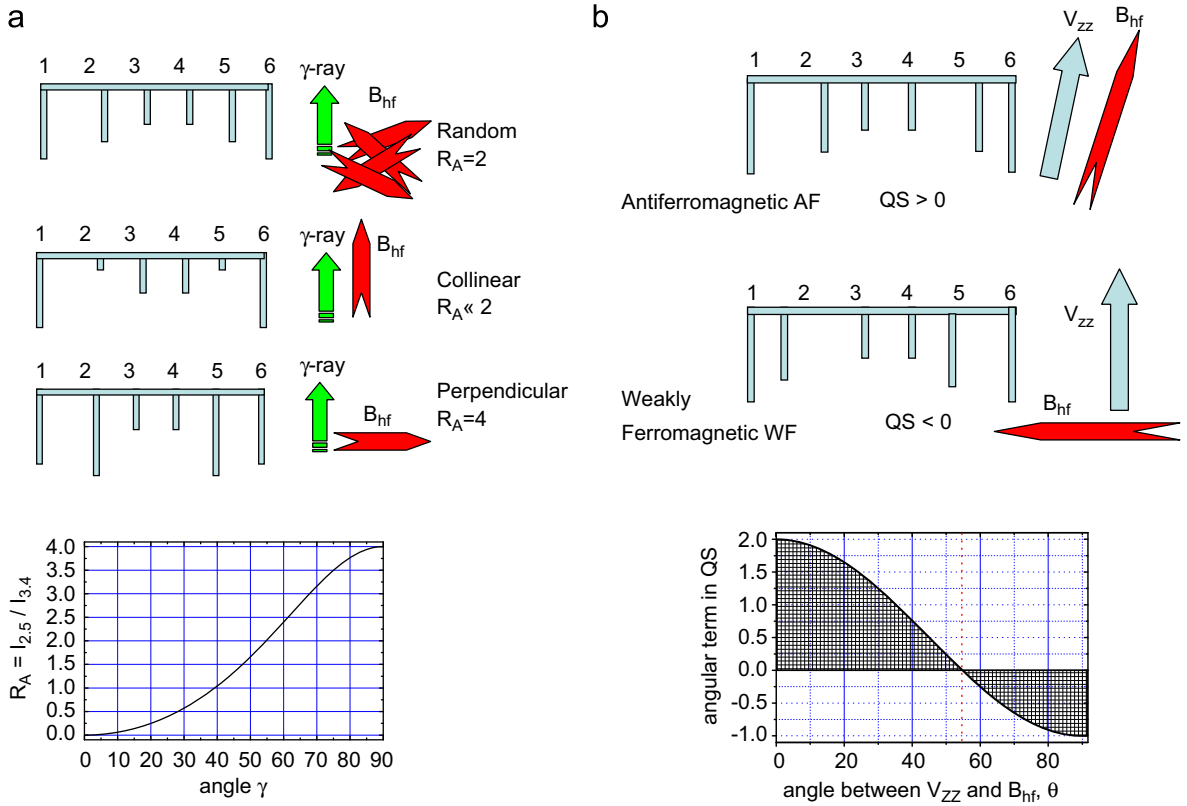

Fig. 6. Cartoon depicting (a) relative line intensities and the relation between B_{hf} direction with respect to γ-ray beam direction. (b) *QS* parameter values and associated line positions and the relation between V_{zz} and B_{hf}.

of opposite sign and with different temperature dependencies [21,27]. At $T > T_M$, K_{MD} dominates, and spins are aligned perpendicular to the *c*-axis (i.e., in the basal plane) in the hexagonal setting. Spins in adjacent layers stacked along the *c*-axis are slightly canted toward each other and a weak ferromagnetic (WF) moment develops in the basal plane [28]. At $T < T_M$, K_{MC} dominates, and spins align along the *c*-axis. and the system is a collinear antiferromagnet (AF) [29,30]. The transition temperature T_M is known to be quite sensitive to the presence of impurities and small particle size. It is obviously pressure dependent. This has been well documented in comparatively low pressure studies to ~10 GPa of early research on pressurized hematite as starting material and in fact T_M rises to room temperature by ~5 GPa. [21] This means that at $P > 5$ GPa at

room temperature, moments start to align along the *c*-axis in an AF configuration of adjacent layers. Neutron diffraction work both at ambient conditions and in a separate study up to ~10 GPa suggests that the spin direction in the sub-lattices of the AF state (at $T < T_M$) are inclined by not more than ~20° away from the *c*-axis [20,31]. At room temperature and the very high pressures reached in our investigation, ~30 GPa at which $T \ll T_M$, it is anticipated that the spins are even closer aligned to the *c*-axis, if not collinear with it.

Therefore in the pressure transformed hematite onset at 13–16 GPa, for which $R_A \leq 1$, it may be inferred from Eq. (1) that the spin direction with respect to the load axis is $\gamma \leq 40°$, see Fig. 6(a). There is thus preferred orientation of the magnetic moments (spin texture) in the load axis direction, consistent with the crystallographic texture seen in the XRD study. This persists to the highest pressure of ~30 GPa, depicted in Fig. 7. It should be noted that such preferred orientation effects are not evident in the low pressure maghemite phase for which $R_A \geq 1.6$. At the highest pressure of 30 GPa where full conversion to the hematite phase is completed $R_A = 1.0$; thus spins are aligned at a 40° (cone) angle to the load axis direction [24]. This spin alignment persists upon decompression to ~7 GPa, see Fig. 7.

Upon decompression to ambient conditions there is an increase in intensity of lines 2 and 5 relative to the innermost lines 3 and 4. A value of $R_A \approx 2.1$ is obtained from the fitting. This means that the moments are either randomly oriented or re-aligned at an angle of $\gamma \approx 55°$ to the load axis (Fig. 6(a)). This spin alignment (magnetic texturing) behavior of the pressure transformed hematite needs to be considered in conjunction with the XRD results which evidence appreciable lattice preferred orientation (crystallographic texture) effects. This will be discussed in the next Section 4.

3.2.3. *Quadrupole shift parameter and spin reorientation*

Since spin alignment features appear to be important in the pressurized sample, another important fitting parameter related to this is the quadrupole shift (*QS*) parameter. This is the interaction of the electric field gradient (EFG) as a result of the local (electronic and nearest neighbor atoms) charge environment and the quadrupole moment. It reflects the site asymmetry of the ^{57}Fe local environment. The expression for *QS* of a magnetically ordered sample in which there is a magnetic hyperfine field B_{hf} at the ^{57}Fe nucleus is given by (see Kolk, pp. 43–44) [26]:

$$QS = \tfrac{1}{8} e^2 qQ (3\cos^2\theta - 1 + \eta^2 \sin^2\theta \cos 2\phi). \quad (2a)$$

where *e* is the electron charge and $eq \equiv V_{zz} = \partial^2 V/\partial z \partial z$ is the maximum value of the EFG in the principle axis system (in which the EFG tensor is diagonal), *V* is the electric potential at the nuclear site, and the *Q* on the right hand side of the equation is the nuclear quadrupole moment of the ^{57}Fe nucleus. The asymmetry parameter $\eta = [V_{xx} - V_{yy}]/V_{zz}$ has values $0 \leq \eta \leq 1$. The angular factor in Eq. (2) involves the polar angles θ and ϕ that B_{hf} makes with the direction of V_{zz}. This *QS* parameter has the effect of shifting each of the resonance lines such that they are not symmetrically centered around zero of velocity on the *x*-scale (see Fig. 6(b)).

The *QS* parameter is only pertinent to hematite whose primitive unit cell (rhombohedral) has lower than cubic symmetry. In the case of hematite, at ambient conditions, V_{zz} is directed along the *c*-axis in the coordinates of the hexagonal unit cell (equivalent [1 1 1] direction in the rhombohedral setting). This is the trigonal axis of the FeO_6 octahedron along which there is axial symmetry and thus $\eta = 0$ in Eq. (2) [21]. The expression for the *QS* thus reduces to

$$QS = \tfrac{1}{8} e^2 qQ (3\cos^2\theta - 1). \quad (2b)$$

The *QS* parameter for the maghemite phase is usually expected to be zero because of the cubic lattice symmetry of the spinel ($V_{zz} = 0$). The Fe atoms having nearest neighbor vacancies contribute slight resonance line broadening effects and normally *QS* is set to zero in fitting spectra of the cubic lattice symmetry situation of the spinel [32]. Recently it has been demonstrated that the presence of nearest neighbor vacancies at the Fe sites in the structure can render the *QS* to be finite [33]. Therefore this can be modeled in high resolution MS spectra of maghemite. However additional line-broadening effects from the ^{57}Co(Rh) source of high specific activity, which is an imperative for the high pressure MS experiments, would render such a detailed analysis unreliable in our case. Slight pressure gradients and deviatoric stresses due to a degree of non-hydrostaticity would also cause some line broadening. Therefore in our analysis of the maghemite spectra $QS \approx 0$ mm/s and resonance line broadening accounts for any site asymmetry effects from the vacancies [4].

In hematite the spin reorientation through T_M is manifested in the angular factor in the *QS* of Eq. (2b), such that *QS* ($\theta \approx 90°$) = −0.20 mm/s for $T > T_M$. This is about half the value and of opposite sign to the case of *QS* ($\theta \approx 0°$) = 0.40 mm/s for $T < T_M$, see also Fig. 6(b) [21]. The *QS* parameter is thus often used to determine whether hematite is in the spin canted WF state or collinear AF state.

In this work the *QS* parameter will prove useful in ascertaining, in the pressure transformed hematite phase, how the spin moments (B_{hf}) align with respect to V_{zz} from Eq. (2b). At ambient pressure this component of the EFG is biased along the crystallographic *c*-axis (which coincides with the trigonal axis of the FeO_6 octahedron). This is in addition to monitoring how the spins align relative to the load axis using the relative absorption intensities and Eq. (1).

The evolution of the *QS* parameter is represented in the labels of Figs. 7 and 8 and is similar to that of a previous study. [4] As soon as hematite becomes the majority phase at $P \geq 19$ GPa the *QS* values increase monotonically from +0.40 mm/s to +0.50 mm/s at 30 GPa, in comparison to $QS \approx -0.20$ mm/s in

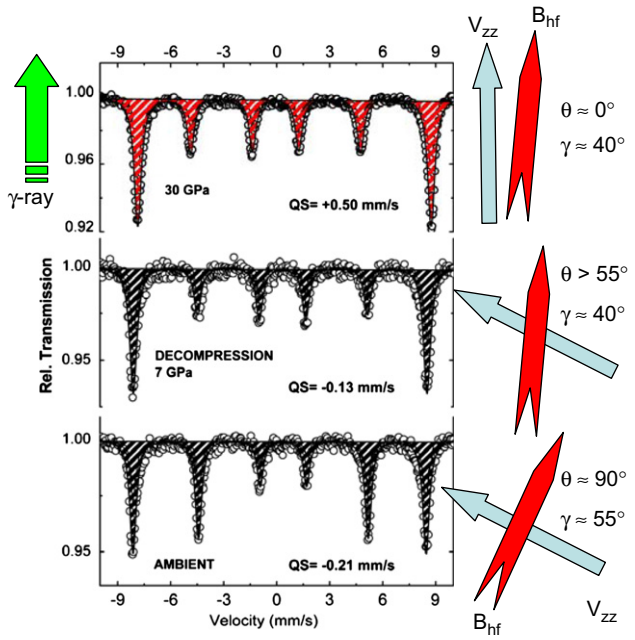

Fig. 7. Mössbauer spectrum at the highest pressure as well as those taken upon decompression. Depiction of the relative orientations of, γ-ray beam, V_{zz} and B_{hf} are also indicated. This is deduced from the *QS* value and ratio R_A, assuming that axial symmetry is maintained throughout. The γ-ray beam coincides with the compression (load axis). The angle between the γ-ray beam and B_{hf} is γ. The angle between V_{zz} and B_{hf} is θ.

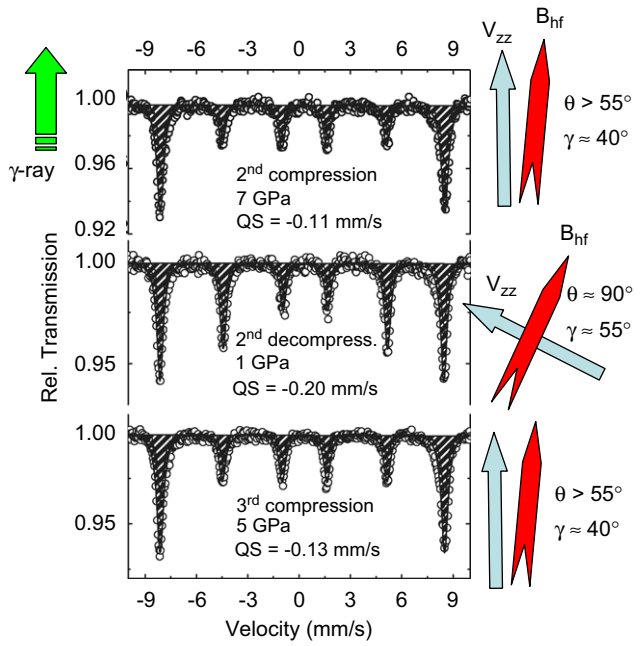

Fig. 8. Mössbauer spectra of decompression–recompression cycles of pressure transformed hematite.

the canted WF state at $P<5$ GPa. The monotonic increase of QS upon rising pressure is likely due to changes in V_{zz} because of changes in inter-atomic distances. The QS values of the pressure transformed hematite are indicative of the collinear AF state similar to the value of hematite starting material below the Morin transition $T<T_M$. At these high pressures T_M is well above room temperature [21]. Recall that from the neutron diffraction pressure study it is anticipated that the spins are aligned at less than 20° to the c-axis, if not collinear with it [31].

3.2.4. Decompression data and recompression

In the decompression sequence from 30 GPa the DAC was decompressed in small pressure steps; however, a Mössbauer spectrum was first recorded when the pressure was as low as ~7 GPa. The QS is seen to be negative indicative of spins at an angle $\theta>55°$ to V_{zz}, see Fig. 6(b). This would be considered as an approach toward the canted WF state, similar to hematite starting material at ambient pressure in which $V_{zz}\perp B_{hf}$. However note that $R_A\approx 1$ in the pressure transformed sample decompressed to ~7 GPa. This is similar to that at the highest pressure indicating that spin alignment is still biased along the load axis, see Fig. 7.

Thus the spins remain aligned close to the load axis ($\gamma\approx 40°$) as it was at ~30 GPa. According to the XRD decompression data this is also the bias direction of the c-axis, as was the case at the highest pressure. Yet the QS value has changed sign compared to the high pressure value. This indicates that the angle θ between B_{hf} and V_{zz} undergoes some change compared to the highest pressure situation. It is not due to a reorientation of B_{hf}, as the R_A value has not changed. The change in QS must rather be ascribed to changes in the EFG (V_{zz}), that is, in the angular factor in Eq. (2) as will be discussed further in the next section.

After decompression to ambient conditions, the anvils were slightly separated from the gasketed sample cavity and the sample left to relax for a few hours. Measurement of this sample still compacted in the gasket cavity, yielded $QS=-0.21$ mm/s (and $R_A\sim 2.1$) typical of hematite starting materials at room temperature where B_{hf} is at 90° to V_{zz}.

Following this recovery to ambient conditions, the sample was recompressed and decompressed to ambient conditions in subsequent sequences. Mössbauer spectra were recorded at each pressure step and these are depicted in Fig. 8. However absorption areas are quite different from the case of randomly oriented magnetic moments [4]. The ratio R_A reverts to the value that occurred at very high pressure in the pressure-induced transformation sequence, $R_A\sim 1$. This is indicative of magnetic moments (B_{hf}) again aligned close to the load axis, $\gamma\sim 40°$. We have not performed pressure XRD studies on the recompressed sample. The Mössbauer data (R_A values) do seem to suggest that c-axis preferred orientation along the load axis persists again in any recompression experiments.

4. Discussion

4.1. Nature of the maghemite to hematite phase transformation

Our XRD pressure studies evidence lattice preferred orientation arising out of the maghemite→hematite transformation. It confirms what has been seen (but not identified as such) recently in pressure studies of a vacancy disordered maghemite starting material [19]. It is perhaps important to note that when hematite is pressurized as a starting material from the outset, this lattice preferred orientation does not seem to occur even to the highest pressures typical of our study [4,5,7]. This is then suggestive that the lattice preferred orientation is linked to the maghemite→hematite structural transformation, although it may also be additionally driven by deviations from hydrostatic stress conditions at these high pressures. Possible future experiments should investigate the transformation when near ideal hydrostatic conditions can be maintained at such elevated pressures, e.g., by using a helium pressure transmitting medium.

The behavior of the maghemite→hematite transition may be compared with the pressure transformation of Fe metal. This undergoes an analogous cubic (bcc)→hexagonal (hcp) lattice structural transformation and has been studied quite extensively because of geophysical implications [34,35]. It has been shown that the α-Fe develops preferred orientation under non-hydrostatic stress conditions [35]. The preferred orientation of the α-phase is inherited by the ε-phase (hcp) in accordance with the Burgers orientation relationship. This is a relationship established by Burgers [36], in which $(1\,1\,0)_{bcc}$ planes would become $(0\,0\,0\,1)_{hex}$ basal planes in a martensitic transformation, because of the structural relationship between bcc and hcp lattices [35]. After the phase transition the ε-phase displays a texture with the c-axis oriented in a direction orthogonal to the load axis direction. Upon further compression the c-axes rotate and become parallel to the load axis.

In our case, the maghemite does not seem to show a high degree of lattice preferred orientation up to the onset of the structural transition during compression. At least it is not as pronounced as what it is in the high pressure transformed hematite. This is deduced from the relative line intensities of both the XRD and Mössbauer spectra up to ~13 GPa near the onset of the phase transition, see figs. 1 and 5. These line intensities (or absorption areas) evolve from R_A values of ~1.8 to ~1.6 at the onset of the structural transition, compared with $R_A\sim 1$ in the pressure transformed sample.

The texture in the pressure transformed hematite may arise from a slip mechanism and a crystallographic plane inherited from the maghemite, as in the bcc→hcp transition of Fe metal, according to a Burgers orientation relationship [35]. Alternatively the transition may be similar to the temperature induced maghemite→hematite transition which proceeds topotactically, meaning that it occurs by a

restacking of various atomic planes rather than by wholesale recrystallization and consequent nucleation and growth [37,38]. It is then supposed that the high pressure phase forms in a crystallographic orientation with the *c*-axis [0 0 0 1] unit cell direction (hexagonal setting) developed along [1 1 1] directions of the cubic spinel unit cell of the low pressure phase [38,39]. In this scenario under compression, it may then be anticipated that *c*-axis alignment along the load axis direction is favored.

4.2. Bulk modulus values

Turning to the mechanical properties of the phases, the bulk modulus of the low and high pressure phases have been calculated by a least-squares fit of the pressure–volume data to a third order Birch–Murnaghan equation of state. The resulting zero-pressure bulk modulus is $B_0=187(\pm4)$ for maghemite and $B_0=268(\pm14)$ GPa for hematite (combining decompression and compression data sets), with an assumption of a pressure derivative $B_0'=4$. The $B_0\sim187$ GPa that we determined for γ-Fe_2O_3 is in good agreement with the values of 190 ± 6 GPa reported by Clark et al. [3] and slightly lower of the values of 203 ± 10 GPa and 213 ± 10 reported by Jiang et al. [2] and Zhu et al. [19], respectively. It seems to be systematically lower than all previously reported B_0 values, perhaps as a result of the vacancy ordered superstructure. The $B_0\sim268$ GPa of our high-density α-Fe_2O_3 is somewhat higher than those of samples reported in the literature [2,7], namely $B_0\sim230$ GPa. Clark et al. report a value of 299 (±30) GPa [3].

4.3. Decompression behavior

Upon decompression to ~7 GPa the magnetic moments remain pinned along the same angle to the load axis ($\sim40^\circ$) as at the highest pressure. Recall that upon decompression the *c*-axis of the hexagonal unit cell also shows preferred orientation along the load axis, see Fig. 2. All of this is deduced from the relative intensities of the spectral lines in both the Mössbauer and XRD data, which do not change from the values at the highest pressure.

There is a need to understand the Mössbauer decompression data at ~7 GPa where the $QS=-0.13$ mm/s has changed sign. This must be due to the angular factor in Eq. (2), indicating that V_{zz} is changing direction or there is a change from axial symmetry (η value affected) or both. Therefore upon decompression to ~7 GPa it is the EFG that is affected and not the B_{hf} orientation. Assuming that axial asymmetry is retained ($\eta=0$), Eq. (2b), the change in sign of the *QS* value is suggestive of V_{zz} becoming orthogonal to B_{hf}. The negative value of the *QS* indicates that $\theta>55^\circ$ at this low pressure, see Fig. 7.

This is likely due to a distortion of the FeO_6 octahedron. A detailed study of the compressional behavior of hematite pressurized as starting material [7], shows that such bond distortions do occur in this material. It is anticipated that this is happening in the decompression of highly textured hematite of this study. A hint of this is found in the behavior of the *c*/*a* ratio plotted in Fig. 3, which has a compelling indication of a discontinuous change onset at ~7 GPa of the decompression sequence.

Upon further decompression to ambient conditions the XRD patterns show that the hematite crystallites remain highly textured as anticipated for a compacted material (with *c*-axis preferred orientation along the load axis), but the magnetic moments swing further away from the load axis (to $\sim55^\circ$) as inferred from the ratio $R_A\approx2$, see Fig. 6(a). Thus from high pressure down to ambient conditions the spin reorientation is only of the order of 15°. Therefore moments cannot be in the basal plane of the hexagonal unit cell if they were aligned close to the *c*-axis at the highest pressure in the AF state as anticipated [31]. Recall that this basal plane orientation is the case in hematite starting material at ambient conditions. This is also what is interpreted to be the case in pressurized hematite starting materials which have been decompressed to ambient conditions [4]. In the recovered sample, Fig. 7, the value $QS=-0.20$ mm/s is suggestive of the moments now being near orthogonal to V_{zz}. We have already indicated that V_{zz} is not necessarily along the same direction it was at high pressure (which was presumably along the *c*-axis), as implied by the behavior of *c*/*a* in Fig. 3 which hints at local structural distortions of the FeO_6 octahedron.

4.4. Recompression behavior of pressure transformed hematite

Turning to the recompression experiments (Fig. 8) we see that there is a change from $R_A\approx2$ at or near ambient pressure to $R_A\approx1$ at ~5 GPa in successive recompression–decompression cycles. Presumably the sample is compacted and remains textured after the first decompression to ambient conditions. This change in the R_A ratio suggests a spin re-alignment of only 15° (with respect to the load axis), Fig. 6(a).

It appears that in the pressure transformed hematite the known 90° spin reorientation of hematite starting material, associated with the Morin transition, is inhibited over wide decompression and recompression ranges. It is suggested that this is due to retained residual strain in the pressure transformed hematite as a result of, or in combination with, defects or crystal imperfections in the material associated with the maghemite→hematite inversion. Similar effects have been seen in shocked hematite or as a function of nanophase grain size [40,41]. Although in those cases it is the WF canted state (basal plane alignment) that is stabilised, in which T_M is suppressed to lower temperatures from ~250 K in hematite starting material at ambient conditions. This transition is very sensitive to crystal imperfections because of how they change the magnetic anisotropy energies that drive the Morin transition [39,41,42].

5. Conclusion

In the pressure transformed phase a high degree of lattice preferred orientation is evident, in contrast to the low pressure maghemite phase. There is crystallographic *c*-axis alignment and an associated magnetic texturing of moments, biased in the direction of the load axis. Decompression data from XRD evidence deformation of the local atomic environment of the Fe atom. This is expected to affect the direction of the maximum value of the electric field gradient (EFG), normally assumed to always be directed along the *c*-axis of the hexagonal unit cell.

Such a well textured hematite sample, likely arising out of the topotactic structural transition allows us to obtain some information on the pressure-response of the spin reorientation behavior. Hematite pressurized as starting material at room temperature shows spin reorientation from basal plane to near *c*-axis alignment occurring over a wide compression range, that is, spin reorientation of $\sim90^\circ$ [4,21]. This corresponds to a rise in the Morin temperature to above room temperature. It is presumed that upon decompression the same re-alignment occurs (nearly 90° spin reorientation) but along a different pressure pathway. The previous ^{57}Fe MS study of maghemite pressure transformed to hematite presumed the same scenario [4].

However, in this study we benefit more information from both the crystallographic and magnetic texture effects revealed in the XRD and MS patterns of the same sample. This shows that such a complete spin reorientation does not seem to occur in the high pressure transformed hematite when it is reverted back to ambient conditions and when it is recompressed back to high

pressures. Spin reorientation seems to be restricted to $\sim 15^{\circ}$ and changes of the MS parameters are rather suggestive of an alteration of the direction of V_{zz}, due to local structural distortions (of the FeO_6 octahedron).

A combination of effects of retained residual lattice strain and crystal imperfections arise out of the pressure-induced structural transformation. These are supposed to account for the strong out of plane component of the spins in the hematite sample recovered to ambient conditions. The residual lattice strain or crystal imperfections, or both effects, possibly originate from the defective (vacancy ordered or disordered) cubic spinel low pressure phase. In temperature transformed samples such vacancies will diffuse out and play no further role. By contrast, under externally applied stress it is conceivable that such remnant defects would remain trapped within the lattice of the high pressure phase. They affect spin reorientation behavior and possibly also the structural pressure-response of the FeO_6 octahedral environment, in comparison to defect-free hematite. The absence of superstructure peaks in the XRD pattern of this pressure transformed hematite suggests that these entrapped defects (vacancies) are disordered within the corundum lattice.

Acknowledgments

We thank E. Boldyreva and S.V. Tsybulya of the Chemistry divisions at Novosibirsk State University for supplying the sample. S.R. Naidoo assisted with the XRD work. This work also profited from beam time provided by ELETTRA to an ICTP funded program for developing nations. Funding has been derived from both the NRF-SA and FRC-UJ (Science) initiatives.

References

[1] F. Baudelet, S. Pascarelli, O. Mathon, J.-P. Itié, A. Polian, J.-C. Chervin, Phys. Rev. B 82 (2010). 140412 (1–4).
[2] J.Z. Jiang, J.S. Olsen, L. Gerward, S. Morup, Europhys. Lett. 44 (1998) 620.
[3] S.M. Clark, S.G. Prilliman, C.K. Erdonmez, A.P. Alivisatos, Nanotech 16 (2008) 2813–2818.
[4] T. Kawakami, S. Nasu, T. Tsutsui, T. Sasaki, T. Yamada, S. Endo, M. Takano, T. Katamoto, J. Phys. Soc. Jpn. 72 (2003) 2640–2645.
[5] S. Ono, K. Funakoshi, Y. Ohishi, E. Takahashi, J. Phys.: Condens. Matter 17 (2005) 269–276.
[6] M.P. Pasternak, G.K. Rozenberg, G.Y. Machavariani, O. Naaman, R.D. Taylor, R. Jeanloz, Phys. Rev. Lett. 82 (1999) 4663–4666.
[7] G.K. Rozenberg, L.S. Dubrovinsky, M.P. Pasternak, O. Naaman, T.L. Bihan, R. Ahuja, Phys. Rev. B 65 (2002). 064112 (1–8).
[8] J. Badro, G. Fiquet, V.V. Struzhkin, M. Somayazulu, H.K. Mao, G. Shen, T.L. Bihan, Phys. Rev. Lett. 89 (2002). 205504 (1–4).
[9] I.S. Lyubutin, A.G. Gavriliuk, Phys. Usp. 52 (2009) 989–1017.
[10] A.N. Shmakov, G.N. Kryukova, S.V. Tsybulya, A.L. Chuvilin, L.P. Solovyeva, J. Appl. Cryst. 28 (1995) 141–145.
[11] A. Hammersley, Comput. Prog. FIT2D (ESRF, Grenoble 1998).
[12] A.C. Larson, R.B.V. Dreele, General Structure Analysis System (GSAS), Los Alamos National Lab Report LAUR 86-748.
[13] S. Takele, G.R. Hearne, Nucl. Instrum. Methods B 183 (2001) 413–418.
[14] R.A. Brand, WinNormos-for-Igor Users Manual, WissEl GmbH, Starnberg, Universität Duisburg, Duisburg, 2006.
[15] G.T. Long, T.E. Cranshaw, G. Longworth, Möss. Effect. Ref. Data J 6 (1983) 42–49.
[16] R. Grau-Crespo, A.Y. Al-Baitai, I. Saadoune, N.H.D. Leeuw, J. Phys.: Condens. Matter 22 (2010). 255401 (1–8).
[17] C. Greaves, J. Solid State Chem 49 (1983) 325–333.
[18] J.-E. Jørgensen, L. Mosegaard, L.E. Thomse, T.R. Jensen, J.C. Hanson, J. Solid State Chem. 180 (2007) 180–185.
[19] H. Zhu, Y. Ma, H. Yang, C. Ji, D. Hou, L. Guo, J. Phys. Chem. Solids 71 (2010) 1183–1186.
[20] A.H. Hill, F. Jiao, P.G. Bruce, A. Harrison, W. Kockelmann, C. Ritter, Chem. Mater. 20 (2008) 4891–4899.
[21] C.L. Bruzzone, R. Ingalls, Phys. Rev. B 28 (1983) 2430–2440.
[22] W.A. Dollase, J. Appl. Crystallogr. 19 (1986) 267–272.
[23] S.-J. Lee, S. Lee, New J. Phys. 8 (2006) 98. doi:10.1088/1367-2630/8/6/098.
[24] U. Gonser, M. Ron, H. Ruppersberg, W. Kuene, A. Trautwein, Phys. Stat. Sol. (a) 10 (1972) 493–499.
[25] H.-D. Pfannes, U. Gonser, Appl. Phys 1 (1973) 93–102.
[26] B. Kolk, Studies of Dynamical Properties of Solids with the Mössbauer Effect, Elsevier, Amsterdam, 1984.
[27] J.O. Artman, J.C. Murphy, S. Foner, Phys. Rev. 138 (1965) 912–917.
[28] F. Bødker, M.F. Hansen, C.B. Koch, K. Lefmann, S. Mørup, Phys. Rev. B 61 (2000) 6826–6838.
[29] R.J. Harrison, S.A. McEnroe, P. Robinson, C.J. Howard, Am. Mineral. 95 (2010) 974–979.
[30] A.H. Morrish, Canted Antiferromagnetism: Hematite, World Scientific, Singapore, 1994.
[31] J.B. Parise, D.R. Locke, C.A. Tulk, I. Swainson, L. Cranswick, Physica B 385–386 (2006) 391–393.
[32] H.A. Annersten, S.S. Hafner, Z. Kristall. B 137 (1973) 320–340.
[33] K.M. Spiers, D.M. Paganin, J.D. Cashion, J. Phys.: Condens. Matter 23 (2011) 1–6.
[34] H.-R. Wenk, S. Matthies, R.J. Hemley, H.-K. Mao, J. Shu, Nature 405 (2000) 1044–1047.
[35] S. Merkel, H.-R. Wenk, P. Gillet, H.-K. Mao, R.J. Hemley, Phys. Earth Planet. Inter. 145 (2004) 239–251.
[36] M.I. Burgers, Physica 1 (1934) 561–586.
[37] J.D. Bernal, D.R. Dasgupta, A.L. Mackay, Nature 180 (1957) 645–647.
[38] S. Kachi, K. Momiyama, S. Shimizu, J. Phys. Soc. Jpn. 18 (1963) 106–116.
[39] D.J. Dunlop, Ö. Özdemir, Rock Magnetism: Fundamentals and Frontiers, Cambridge University Press, Cambridge, 1997.
[40] D.L. Williamson, E.L. Venturini, R.A. Graham, B. Morosin, Phys. Rev. B 34 (1986) 1899–1907.
[41] Ö. Özdemir, D.J. Dunlop, T.S. Berquó, Geochem. Geophys. Geosys. 9 (2008) Q10Z01. doi:10.1029/2008GC002110.
[42] O. Özdemir, D.J. Dunlop, J. Geophys. Res. 111 (2006). B12S03 (1–13).